Research paper

Comparative study of hydrogen storage on metal doped mesoporous materials

P.M. Carraro [a,b], K. Sapag [c], M.I. Oliva [b], G.A. Eimer [a,*]

[a] CITeQ (CONICET – UTN), Maestro López y Cruz Roja Argentina, Ciudad Universitaria, 5016 Córdoba, Argentina
[b] IFEG (CONICET – UNC), Medina Allende, Ciudad Universitaria, 5016 Córdoba, Argentina
[c] Laboratorio de Sólidos Porosos (INFAP – CONICET – UNSL), Ejército de los Andes 950, 5700 San Luis, Argentina

ARTICLE INFO

ABSTRACT

The hydrogen adsorption capacity of mesoporous materials MCM-41 modified with Co, Fe, Ti, Mg and Ni at 77 K and 10 bar was investigated. Various techniques including XRD, N_2 adsorption and DRUV–vis were employed for the materials characterization. The results showed that a low nickel loading on MCM-41 support promoted the presence of hydrogen-favorable sites, increasing the hydrogen storage capacity.

1. Introduction

Hydrogen has drawn attention as a next-generation energy carrier for mobile and stationary power sources. To achieve economic feasibility, hydrogen storage materials with high gravimetric and volumetric densities must be developed [1]. The utilization of nanotechnology appears to be an efficient strategy to address the challenges mentioned above [2]. Metal hydrides or complex hydrides, metal organic frameworks (MOFs), nanoporous materials have attract the attention of the researchers for hydrogen storage applications [3–5]. Among them, porous silicon has been examined as hydrogen storage system [6]. In addition, several scientists have fabricated hybrid systems based on carbon nanotube (SWCNT) and porous silicon. In order to improve the hydrogen storage, the metal doping on nanostructured materials would improve the strength of interactions through chemisorption [6–8]. One of main disadvantages of chemical adsorption is the high temperatures for release the hydrogen stored [6]. Therefore, the physisorption provides an important alternative to be applied to transport. The main advantage is the reversibility and kinetic rapidity of hydrogen adsorption compared to chemical adsorption. However, the main problem is the low enthalpy of adsorption, which results in a low storage capacity under environmental conditions. Therefore, nanostructured mesoporous materials are attractive as adsorbents for physisorption storage systems. The increased surface area and porosity of nanostructures afford additional binding sites on the surface and in the pores that can improve the storage mainly through physical adsorption. Mesoporous molecular sieves of the MCM-41 type have some attributes, which are desirable for hydrogen storage applications, such as their high specific surface and high capacity to functionalize its surface [3]. An alternate approach to increase the hydrogen storage capacity of mesoporous nanomaterials is by doping them with different metals [5,9]. Nevertheless, the metal loading on MCM-41 support must to be optimized because of that higher concentrations of metals produces the structural collapse of the mesoporous silica framework, decreasing the hydrogen adsorption, as previously was reported by us and others authors [5,9–11]. Thus, it is interesting to compare the affinity for hydrogen of different metals modified mesoporus materials to be used as hydrogen storage systems.

In this work, a comparative study of siliceous mesoporous materials MCM-41 modified with different metals (Co, Fe, Ti, Mg, Ni and 2.5 wt% metal content) as possible candidates to hydrogen storage was presented. Their textural, structural and chemical properties were characterized and the hydrogen adsorption data interpreted according to the properties of theses mesoporous materials.

2. Material and methods

2.1. Samples preparation

The pure siliceous mesoporous material (MCM-41) was synthesized as previously reported [12]. The precursors used for the modification of the MCM-41 host with metals (metal loading

* Corresponding author.
  E-mail address: geimer@frc.utn.edu.ar (G.A. Eimer).

2.5 wt%) were: $Co(NO_3)_2 \cdot 6H_2O$ (Riedel-de Haën 98%), $Fe(NO_3)_3 \cdot 9H_2O$ (Aldrich 98%), titanium n-butoxide (Fluka 97%) in iso-propanol (Cicarelli 99.5%), $Mg(NO_3)_2 \cdot 6H_2O$ (Anedra 99%) and $Ni(NO_3)_2 \cdot 6H_2O$ (Merck pro analysis). Incipient impregnation was performed using an appropriate amount of the precursor aqueous solution. Subsequently, the water was slowly removed by rotary evaporation at 323 K for about 30 min. The resulting powder was dried at 333 K for 12 h and finally calcined for 9 h at 773 K. The synthesized materials were named as follows: Fe/MCM-41, Co/MCM-41, Ti/MCM-41, Mg/MCM-41 and Ni/MCM-41.

2.2. Characterization

The structural characterization of the samples was performed by X-ray diffraction (XRD) using in PANanalytical Empyrean diffractometer with Cu Kα radiation (λ = 1.5418 Å) in the range of 2θ from 0.7° to 7°. The textural characterization was carried out by N_2 adsorption–desorption isotherms at 77 K (N_2 with 99.999% purity) conducted in an ASAP 2000 (Micromeritics Instruments). Before the measurements, the samples were vacuum-degassed at 523 K for 12 h under vacuum. The specific surface (S_{BET}) was calculated by the Brunauer-Emmett-Teller (BET) method using the adsorption data, in the pressure range of P/P_0: 0.05–0.25, where the conditions of linearity and considerations regarding the method were fulfilled. The total pore volume (V_{TP}) was obtained by the Gurvich́s rule at a relative pressure of 0.98. The pore size distributions of the samples were determined by NLDFT method for SiO_2 cylindrical pores in the adsorption and desorption branches. The UV–Vis diffuse reflectance spectra (UV–Vis DRS) were recorded in air at room temperature using a Jasco 650 spectrometer with an integrating sphere in the wavelength range of 200–900 nm.

2.3. Hydrogen adsorption

Hydrogen adsorption measurements at 77 K and pressures up to 10 bar were performed in a static volumetric system (Micromeritics Instrument Corporation, USA, ASAP 2050) appropriately calibrated. For the adsorption experiments, high-purity hydrogen gas (99.9999%) was used in the equipment. Before adsorption experiments, samples were degassed at 573 K during 12 h under vacuum conditions (5×10^{-3} mmHg). Helium was used to measure the void volume of the sample cell in both instruments, before each analysis.

3. Results and discussion

3.1. Textural and physico-chemical characterization

Low-angle X-ray diffraction analysis of the MCM-41 sample (Fig. 1) revealed an intense reflection at about a 2θ value of 2.5° assigned to the (1 0 0) diffraction plane, and weak peaks in the 2θ range of 4–5° due to higher order reflection lines attributable to the (1 1 0) and (2 0 0) planes. Thus, the presence of these peaks indicates that the materials fully retain the long-range mesopore ordering, typical of MCM-41 support [12]. Therefore, no significant changes were noticed after metal loading, except for slight shift of the main XRD peak towards higher angles and decrease in the intensity of all peaks. These features can be attributed to some structural deterioration and incorporation of metal species inside the pores, after the metal loading.

Fig. 2 shows the N_2 adsorption–desorption isotherms at 77 K of the MCM-41 support and the samples loaded with Co, Fe, Ti, Mg and Ni. All of the solids exhibit type IV isotherms, typical of well-defined mesoporous structure with a hysteresis loops with parallel and almost horizontal branches, classified as H4-type according to
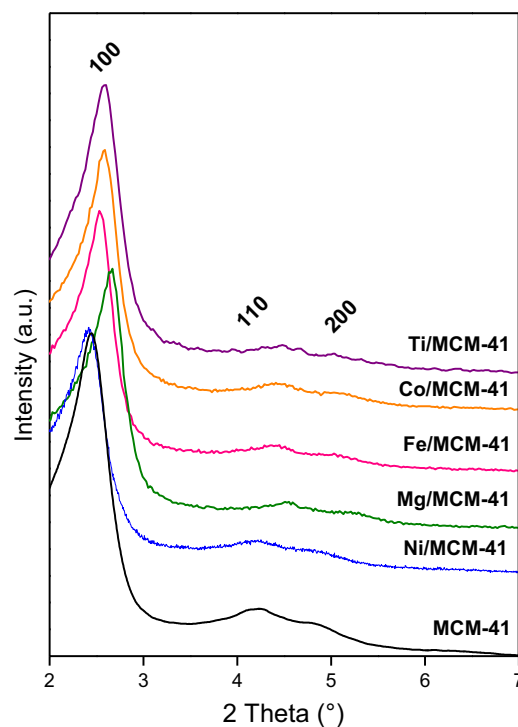

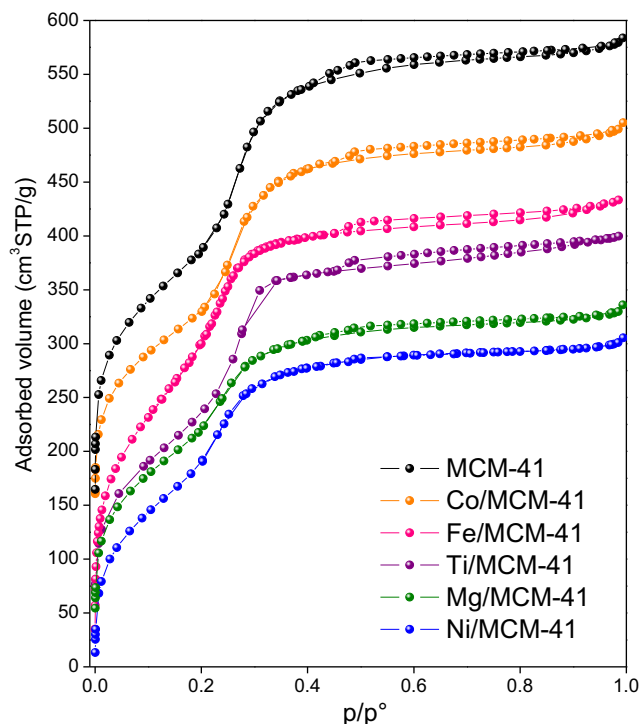**Fig. 1.** Low-angle XRD patterns of the samples.

Fig. 2. N_2 adsorption–desorption isotherm at 77 K of the samples.

IUPAC [13,14]. The metal modified samples show identical shapes with respect to MCM-41 support, indicating that the pore structure has not been significantly affected. In addition, all samples showed a narrow step of capillary condensation in the p/p^0 range from 0.1 to 0.25, providing clear evidence of the narrowly defined mesopore diameter range. It is known that the presence of oxides could affect

the adsorbate-adsorbent interaction and their location could also influence the pores geometry [15].

Table 1 summarizes the textural properties of all resulting materials. Mesoporous materials show average pore sizes around 3 nm, high specific areas and pore volumes typical of MCM-41 structures. These last parameters are slightly decreased with metal nominal loading in comparison with MCM-41 support. This behavior can be attributed to the presence of metal oxide species formed both inside the channels as well as on the external surface, which is also contributing to certain loss of mesostructuration degree. This partial pore blocking by metal oxides is especially notable for some samples and expected for such materials modified with metals by wet impregnation [5,11].

UV–Vis DR spectroscopy is a useful method to understand the coordination environment of transition metals in the MCM-41 type structure [15,16]. The UV–Vis DR spectra of the investigated samples are shown in Fig. 3, where each spectrum differs depending on the metal loaded into the support. For pure MCM-41 sample, there is no absorption peak in the UV–visible region, indicating that it is not sensitive to UV or visible light. However, for Co/MCM-41 sample, a very broad absorption between 200 and 860 nm can be observed. A first band, at around 260 nm, is usually assigned to a charge transfer from the oxygen ligand to Co^{2+} ion in tetrahedral symmetry [15,17]. Meanwhile, absorptions between 300 and 400 nm could be originated from the characteristic electronic transitions of Co^{3+} in disordered tetrahedral environment. On the other hand, the absorption in the 400–600 nm range can be assigned to octahedral Co^{2+} species, such as CoO clusters. Finally, the absorption region between 600 and 800 nm indicates the presence of cobalt oxide nanoparticles in the form of Co_3O_4, where Co^{2+} ions are in tetrahedral coordination and Co^{3+} ions are in octahedral positions [17]. In the case of Fe/MCM-41 sample, three absorption regions at about 200–310, 310–450 and 450–650 nm can be considered. The first maximum at about 254 nm, associated with the $d\pi$–$p\pi$ charge transfer between Fe and O [15,18], indicates that some iron is able to link to O atoms of the framework as isolated Fe^{3+} cations. The bands detected at longer wavelengths, evidence that iron is also present with octahedral coordination in extra-framework positions. Thus, the second absorption region (at about 378 nm) may be ascribed to small oligonuclear clusters, whereas the last absorption (between 450 and 650 nm) may be assigned to larger iron oxide nanoparticles [19]. With respect to the Ti/MCM-41 sample, the absorption band observed in the region of 260–300 nm suggests indicates that most of the Ti species are isolated and in tetrahedral coordination inside the framework that most of the Ti species are isolated and in tetrahedral coordination inside the framework. In addition, compared to the bulk anatase TiO_2, an absorption band at about 300–330 nm could be due to octahedral extra-framework titanium [20]. Meanwhile, for the spectra corresponding to the Mg/MCM-41 sample, an absorption band at about 250 nm is observed, which could be assigned to Mg-O pairs involving 3-coordinated O^{2-} ions [21]. Finally, the Ni/
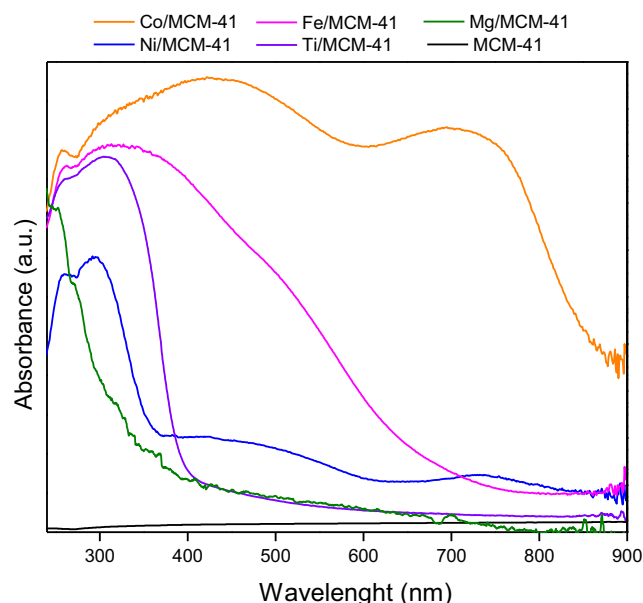

Fig. 3. UV–vis DR spectra of the samples.

MCM-41 sample presents an intense absorption in 250–350 nm range, which is typically associated to the $O^{2-}(2p)\rightarrow Ni^{2+}(3d)$ charge transfer transition of octahedral Ni^{2+} species in NiO lattices [16]. In addition, others absorption bands at about 400–550 and 700–850 nm are observed, which are associated to Ni^{2+} ions in octahedral local environment in NiO [22]. Moreover, the band around at 260 nm could be assigned to the presence of isolated mononuclear Ni^{2+} species interacting with the mesoporous framework oxygen, related to a $O^{2-}\rightarrow Ni^{2+}$ charge transfer transition in the mesoporous lattice.

3.2. Hydrogen adsorption measurements

Fig. 4 displays H_2 adsorption excess isotherms of the different adsorbents at 77 K. It is interesting to note that desorption branches show a good reversibility of hydrogen adsorbed. In addition, a maximum of the Gibbs excess amount in the pressure range is observed for the most samples. This maximum occurs at a point where the difference between the density of the adsorbed phase and the bulk phase is maximal [23]. In the case of these materials, the saturated adsorption capacity is quickly achieved (saturation point of the available adsorption sites), whereby it can be considered that the adsorption sites are few and the storage capacity of these materials is less. This is important to keep in mind when designing materials for the hydrogen storage. As it can be seen, Ni/MCM-41 and Mg/MCM-41 materials are the only samples that does not present this maximum. It is interesting to observe that, at low pressures (up to 1 bar), these samples present similar or less hydrogen storage capacities than the MCM-41 support. However, this behavior is modified at high pressure for Ni/MCM-41. Thus, nickel incorporation into the mesoporous silica framework enhanced the hydrogen sorption capacity at 77 K (reaching a 1.23 wt% around 10 bar) while that Co, Fe, Ti and Mg loadings decreased the adsorption. Taking into account that at liquid nitrogen temperature (77 K) physorption is a dominant mechanism, the textural properties of these materials could be the determining factor in the H_2 storage capacity. However, considering that the textural properties of Ni/MCM-41 sample are similar to those of other metal modified materials, the Ni species finely dispersed would act as hydrogen favorable active sites, playing an important role in hydrogen storage. According to these results, the other metal

Table 1
Textural properties of the synthesized samples.

Sample	S_{BET} (m^{2}g^{-1})[a]	V_{TP} (cm^{3}g^{-1})[b]	D_P (nm)[b]
MCM-41	940	0.70	3.5
Co/MCM-41	862	0.62	3.1
Fe/MCM-41	848	0.68	3.5
Ti/MCM-41	849	0.65	3.5
Mg/MCM-41	825	0.53	3.2
Ni/MCM-41	860	0.54	3.2

[a] Determined by BET.
[b] Pore diameter (Dp) and pore volume (V_{TP}) determined by N_2 adsorption–desorption.
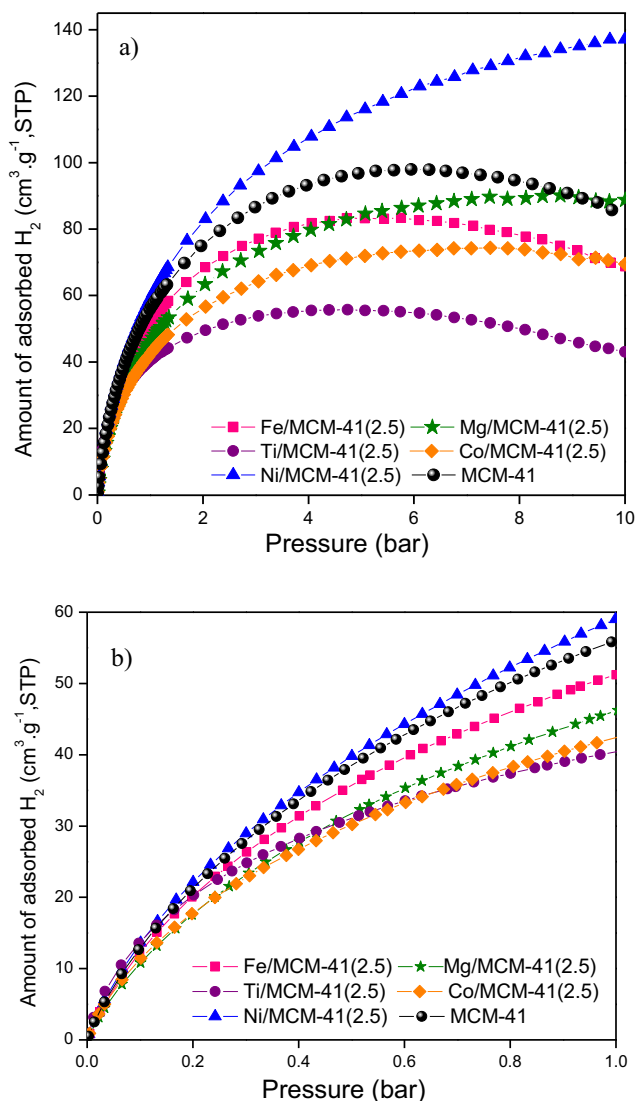
Fig. 4. H$_2$ adsorption–desorption isotherms of the synthesized samples, measured at 77 K (a) and (b) the amplified region for low pressures.
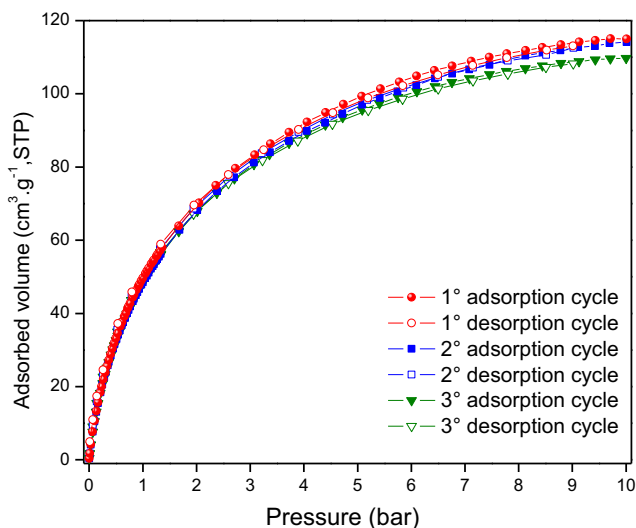

Fig. 5. H$_2$ adsorption–desorption cycles at 77 K and 10 bar of the Ni/MCM-41 sample.

species formed on the support are not perhaps species responsible of the H$_2$ adsorption.

On the other hand, except for Ni, doping of Co, Fe, Mg and Ti on MCM-41 did not contribute to enhance the hydrogen storage of the MCM-41 support. This fact could be due to a major formation of oxide clusters or nanoparticles, which may be avoiding the access of hydrogen towards the interior of channels. It is noteworthy that the MCM-41 support presents the highest specific surface and pore volume, corroborating that the textural properties in these materials (except for Ni/MCM-41) would be determining the H$_2$ storage capacity.

H$_2$ adsorption–desorption cycles of the sample that presented the best performance has been tested in order to demonstrate the ability to retain reversibly hydrogen. Thus, repetitive H$_2$ adsorption–desorption cycles at 77 K and 10 bar of the Ni/MCM-41 sample is display in Fig. 5, in which it can be seen that hydrogen is stored reversibly in this material.

4. Conclusions

MCM-41 mesoporous materials were modified by doping with different metals in order to evaluate the hydrogen storage capacity. All the materials exhibited high specific surface, pore volume and good structural regularity retaining the MCM-41 structure after the metal loading. The presence of different metal species was detected by UV–Vis DRS. Thus, large particles on the external surface as well as nanoparticles and/or clusters of oxides inside the pore channels cause a partial blocking pores. Therefore, except for Ni/MCM-41 material, Co, Fe, Ti and Mg doped mesoporous MCM-41 samples did not contribute to the hydrogen storage. Thus, a low nickel loading favoured a high dispersion of nickel species that promotes affinity towards molecular hydrogen. These results highlight the good performance of nickel on ordered mesoporous supports as promising materials for improving hydrogen storage.

5. Funding

6. Declarations of interest

None.

References

[1] K.T. Møller, T.R. Jensen, E. Akiba, H.-W. Li, Hydrogen – a sustainable energy carrier, Prog Nat. Sci.: Mater. Int. 27 (2017) 34–40, https://doi.org/10.1016/j.pnsc.2016.12.014.

[2] X. Yu, Z. Tang, D. Sun, L. Ouyang, M. Zhu, Recent advances and remaining challenges of nanostructured materials for hydrogen storage applications, Prog. Mater Sci. 88 (2017) 1–48, https://doi.org/10.1016/j.pmatsci.2017.03.001.

[3] D.A. Sheppard, C.E. Buckley, Hydrogen adsorption on porous silica, Int. J. Hydrogen Energy 33 (2008) 1688–1692, https://doi.org/10.1016/j.ijhydene.2007.12.021.

[4] R. Balderas-Xicohténcatl, M. Schlichtenmayer, M. Hirscher, High volumetric hydrogen storage capacity using interpenetrated metal-organic frameworks, Energy Technol. 6 (3) (2017) 510–512, https://doi.org/10.1002/ente.201700636.

[5] K. Prasanth, M. Raj, H. Bajaj, T. Kim, R. Jasra, Hydrogen sorption in transition metal modified ETS-10, Int. J. Hydrogen Energy 35 (2010) 2351–2360, https://doi.org/10.1016/j.ijhydene.2008.10.078.

[6] A.I. Manilov, V.A. Skryshevsky, Hydrogen in porous silicon – a review, Mater. Sci. Eng., B 178 (2013) 942–955, https://doi.org/10.1016/j.mseb.2013.05.001.

[7] H. Ghorbani Shiraz, F. Razi Astaraei, S. Fardindoost, Z. Sadat Hosseini, Decorated CNT based-on porous silicon for hydrogen gas sensing at room temperature, RSC Adv. 6 (2016) 44410–44414. http://10.1039/C6RA03541H.

[8] P. Kale, A.C. Gangal, R. Edla, P. Sharma, Investigation of hydrogen storage behavior of silicon nanoparticles, Int. J. Hydrogen Energy 37 (2012) 3741–3747, https://doi.org/10.1016/j.ijhydene.2011.04.054.

[9] C. Wu, Q. Gao, J. Hu, Z. Chen, W. Shi, Rapid preparation, characterization and hydrogen storage properties of pure and metal ions doped mesoporous MCM-41, Micropor. Mesopor. Mater. 117 (2009) 165–169, https://doi.org/10.1016/j.micromeso.2008.06.020.

[10] M. Zielinski, R. Wojcieszak, S. Monteverdi, M. Mercy, M.M. Bettahar, Hydrogen storage in nickel catalysts supported on activated carbon, Int. J. Hydrogen Energy 32 (2007) 1024–1032, https://doi.org/10.1016/j.ijhydene.2006.07.004.

[11] P.M. Carraro, V.R. Elías, A.A. García Blanco, K. Sapag, S. Moreno, M.I. Oliva, G.A. Eimer, Synthesis and multi-technique characterization of nickel loaded MCM-41 as potential hydrogen-storage materials, Micropor. Mesopor. Mater. 191 (2014) 103.

[12] V. Elías, M. Crivello, E. Herrero, S. Casuscelli, G. Eimer, Some considerations to optimize the synthesis procedure and the structural quality of mesostructured silicas, J. Non-Cryst. Solids 355 (2009) 1269–1273, https://doi.org/10.1016/j.jnoncrysol.2009.04.019.

[13] D. H. Everett. Manual of symbols and terminology for physicochemical quantities and units Appendix II. Definitions, terminology and symbols in colloid and surface chemistry. Part I. (1971) (IUPAC).

[14] P.I. Ravikovitch, D. Wei, W.T. Chueh, G.L. Haller, A.V. Neimark, Characterization of micro- and mesoporosity in SBA-15 materials from adsorption data by the NLDFT method, J. Phys. Chem. B 101 (1997) 3671, https://doi.org/10.1021/jp9625321.

[15] V.R. Elías, E.G. Vaschetto, K. Sapag, M. Crivello, S.G. Casuscelli, G.A. Eimer, Synthesis and photocatalytic activity of titania-loaded transition metal-modified MCM-41 molecular sieves, Top. Catal. 54 (2011) 277–286, https://doi.org/10.1007/s11244-011-9658-1.

[16] A. Tirsoaga, D. Visinescu, B. Jurca, A. Ianculescu, O. Carp, Eco-friendly combustion-based synthesis of metal aluminates MAl_2O_4 (M = Ni, Co), J. Nanopart. Res. 13 (2011) 6397–6408, https://doi.org/10.1007/s11051-011-0392-1.

[17] Z.Y. Yuan, T.H. Chen, J.Z. Wang, H.X. Li, Synthesis and characterization of silicon and cobalt substituted mesoporous aluminophosphates, Colloids Surf A 179 (2001) 253–259, https://doi.org/10.1016/S0927-7757(00)00645-2.

[18] A. De Stefanis, S. Kaciulis, L. Pandolfi, Preparation and characterization of Fe-MCM-41 catalysts employed in the degradation of plastic materials, Micropor. Mesopor. Mater 99 (2007) 140–148, https://doi.org/10.1016/j.micromeso.2006.08.033.

[19] S. Liu, Q. Wang, P. Van Der Voort, P. Cool, E. Vansant, M. Jiang, Magnetism of iron-containing MCM-41 spheres, J. Magn. Magn. Mater. 280 (2004) 31–36, https://doi.org/10.1016/j.jmmm.2004.02.019.

[20] V.R. Elías, M.E. Crivello, E.R. Herrero, S.G. Casuscelli, G.A. Eimer, Synthesis of titanium-containing mesoporous silicas as catalysts for cyclohexene epoxidation, Ind. Eng. Chem. Res. 48 (2009) 9076–9082, https://doi.org/10.1021/ie8018017.

[21] W. Janssens, E.V. Makshina, P. Vanelderen, F.D. Clippel, K. Houthoofd, S. Kerkhofs, et al., Ternary $Ag/MgO-SiO_2$ catalysts for the conversion of ethanol into butadiene, Chemsuschem 8 (2015) 994–1008, https://doi.org/10.1002/cssc.201402894.

[22] K. Hadjiivanov, M. Mihaylov, D. Klissurski, P. Stefanov, N. Abadjieva, E. Vassileva, L. Mintchev, Characterization of Ni/SiO_2 catalysts prepared by successive deposition and reduction of Ni^{2+} ions, J. Catal. 185 (1999) 314–323, https://doi.org/10.1006/jcat.1999.2521.

[23] M. Bastos-Neto, C. Patzschke, M. Lange, J. Mollmer, A. Moller, S. Fichtner, C. Schrage, D. Lassig, J. Lincke, R. Staudt, H. Krautscheid, R. Glaser, Assessment of hydrogen storage by physisorption in porous materials, Energy Environ. Sci. 5 (2012) 8294–8303, https://doi.org/10.1039/c2ee22037g.